Supplementary information for:

Mitigating non-radiative decay losses in the Purcell effect at sub-10 nm nanostructure proximities

Mochamad Januar[1], Bei Liu[1], Eric Wei-Guang Diau[2,3], Hiroaki Misawa[3,4], Hui-Hsin Hsiao[5], Min-Hsiung Shih[6], Kuo-Kang Liu[7], Jui-Ching Cheng[8], Koji Hatanaka[6,9,10], Kou-Chen Liu[1,11,12,13*]

[1*]Department of Electronic Engineering, Chang Gung University, Taoyuan, 33302, Taiwan.

[2]Department of Applied Chemistry and Institute of Molecular Science, National Yang Ming Chiao Tung University, Hsinchu, 300093, Taiwan.

[3]Center for Emergent Functional Matter Science, National Yang Ming Chiao Tung University, Hsinchu, 300093, Taiwan.

[4]Research Institute for Electronic Science, Hokkaido University, Sapporo, 001-0021, Japan.

[5]Department of Engineering Science and Ocean Engineering, National Taiwan University, Taipei, 10617, Taiwan.

[6]Research Center for Applied Sciences, Academia Sinica, Taipei, 11529, Taiwan.

[7]School of Engineering, University of Warwick, Coventry, CV4 7AL, United Kingdom.

[8]Department of Electronic Engineering, National Taipei University of Technology, Taipei, 10608, Taiwan.

[9]Research Administration Office, Organization for Research Strategy and Development, Okayama University, Okayama, 700-8530, Japan.

[10]Center for Optical Research and Education (CORE), Utsunomiya University, Tochigi, 321-8585, Japan.

[11]Department of Materials Engineering, Ming Chi University of Technology, New Taipei City, 24301, Taiwan.

[12]Healthy Aging Research Center, Chang Gung University, Taoyuan, 33302, Taiwan.

[13]Division of Pediatric Infectious Disease, Department of Pediatrics, Chang Gung Memorial Hospital, Linkou, 33305, Taiwan.

*Corresponding author(s). E-mail(s): jacobliu@mail.cgu.edu.tw;

S1 Calculation method: Exact theory

A rigorous analytical solution for the decay rate of an electric dipole positioned at a radial distance from the surface of a nonmagnetic spherical nanoparticle (NP) has been previously developed by Ruppin[1] and Kim *et al.*[2]. According to this theory, the enhanced excitation rate, the radiative decay rate, and the total decay rate expressions for an emitter dipole situated outside the spherical NP can be written as[3]:

$$
\begin{aligned}
\frac{\Gamma_{\text{exc}}}{\Gamma^0_{\text{exc}}} &= \frac{1}{(kr)^2}\sum_{\ell=1}^{\infty}\left(\ell+\frac{1}{2}\right)\left\{\ell(\ell+1)\left|\frac{\psi_\ell(kr)-a_\ell\xi_\ell(kr)}{kr}\right|^2|\psi_\ell(kr)-b_\ell\xi_\ell(kr)|^2\right. \\
&\quad \left.+\,|\psi'_\ell(kr)-a_\ell\xi'_\ell(kr)|^2\right\}\ , \\
\frac{\Gamma^{\perp}_{\text{rad}}}{\Gamma^0_{\text{rad}}} &= \frac{3}{2(kr)^4}\sum_{\ell=1}^{\infty}\ell(\ell+1)(2\ell+1)\,|\psi_\ell(kr)-a_\ell\xi_\ell(kr)|^2\ , \\
\frac{\Gamma^{\parallel}_{\text{rad}}}{\Gamma^0_{\text{rad}}} &= \frac{3}{4(kr)^2}\sum_{\ell=1}^{\infty}(2\ell+1)\left(|\psi_\ell(kr)-b_\ell\xi_\ell(kr)|^2+|\psi'_\ell(kr)-a_\ell\xi'_\ell(kr)|^2\right)\ , \\
\frac{\Gamma^{\perp}_{\text{tot}}}{\Gamma^0_{\text{rad}}} &= 1-\frac{3}{2(kr)^4}\sum_{\ell=1}^{\infty}\ell(\ell+1)(2\ell+1)\Re\left[a_\ell\xi^2_\ell(kr)\right] \\
\frac{\Gamma^{\parallel}_{\text{tot}}}{\Gamma^0_{\text{rad}}} &= 1-\frac{3}{4(kr)^2}\sum_{\ell=1}^{\infty}(2\ell+1)\Re\left[a_\ell\xi'^2_\ell(kr)+b_\ell\xi^2_\ell(kr)\right]\ ,
\end{aligned}
\tag{S1}
$$

" $\perp$ " and " $\parallel$ " represent the perpendicular and parallel dipole orientations relative to the NP surface, respectively. The non-radiative decay rate is computed by subtracting the radiative decay rate from the total decay rate for each dipole orientation:

$$
\frac{\Gamma^{\parallel,\perp}_{\text{loss}}}{\Gamma^0_{\text{rad}}} = \frac{\Gamma^{\parallel,\perp}_{\text{tot}}}{\Gamma^0_{\text{rad}}} - \frac{\Gamma^{\parallel,\perp}_{\text{rad}}}{\Gamma^0_{\text{rad}}}\ . \tag{S2}
$$

Following this, the average rate for the decay channels can be computed by using: $\Gamma_{\text{rad,loss}} = \frac{1}{3}(2\Gamma^{\parallel}_{\text{rad,loss}} + \Gamma^{\perp}_{\text{rad,loss}})$. This computation is feasible given that the dipole orientations are two parallel and one perpendicular. In Eq. S1, a_ℓ and b_ℓ are the well-known Mie scattering coefficients[4]. Meanwhile, ψ and ξ are the Riccati-Bessel functions, defined as $\psi_\ell(kr) = krj_\ell(kr)$ and $\xi_\ell(kr) = krh^{(1)}_\ell(kr)$, where j_ℓ and $h^{(1)}_\ell$

are the spherical Bessel functions of the first and third kind, respectively. The prime notation ($\prime$) in the Riccati-Bessel functions signifies the first-order derivative of the argument inside the parentheses. Additionally, k stands for the wavenumber, r is the radial position, and ℓ signifies the multipolar excitation number. The maximum number of ℓ in the summation is set to a large number ($\ell_{\max} = 100$)[5].

With these decay rates, the modified photoluminescence (PL) quantum yield for a dipolar emitter with a known intrinsic quantum yield, Q^0_{PL}, as a function of light frequency, ω, and radial distance, r, can be obtained as[3]:

$$\frac{Q_{\mathrm{PL}}}{Q^0_{\mathrm{PL}}}(\omega, r) = \frac{\frac{\Gamma_{\mathrm{rad}}}{\Gamma^0_{\mathrm{rad}}}(\omega, r)}{1 + Q^0_{\mathrm{PL}}\left(\frac{\Gamma_{\mathrm{rad}}}{\Gamma^0_{\mathrm{rad}}}(\omega, r) + \frac{\Gamma_{\mathrm{loss}}}{\Gamma^0_{\mathrm{rad}}}(\omega, r) - 1\right)} . \tag{S3}$$

The dielectric functions for the metals used in the calculation were sourced from the recently reported experimental optical databases by McPeak for Al[6] and by Johnson and Christy for Au[7].

In NPs, the electron scattering effect becomes prominent when the particle's diameter is comparable to the mean free path of the electrons in the metal. This effect can significantly influence the dielectric properties of the NP. To capture this influence, a correction is applied to the dielectric function of each metal, as stated in Eq. S4.

$$\varepsilon_{\mathrm{NP}} = \varepsilon + \frac{\omega^2_{\mathrm{D}}}{\omega^2 + i\gamma_{\mathrm{D}}\omega} - \frac{\omega^2_{\mathrm{D}}}{\omega^2 + i\gamma_{\mathrm{cor}}\omega} . \tag{S4}$$

In the equation, $\gamma_{\mathrm{cor}} = \gamma_{\mathrm{D}} + \frac{hv_F}{R}$ denotes the Drude damping factor that has been corrected for the mean free path of electrons. The term R, given by $R = \frac{4}{3}r_{\mathrm{NP}}$, signifies the effective mean free path of electrons when scaled by the NP radius r_{NP}. The Fermi velocity of free electrons in metals, represented by v_{F}, varies for different metals: it is 1.448×10^6 ms^{-1} for Ag, 1.382×10^6 ms^{-1} for Au, and 1.599×10^6 ms^{-1} for Al. The constant h refers to Planck's constant.

S2 Quantum yield of various intrinsic qualities of emitting materials

Figure S1 shows the PL quantum yield as a function of the emitter's position relative to the surface of a 60 nm-diameter Al NP, calculated for different intrinsic quantum yields, Q^0_{PL}. Here, $Q^0_{\mathrm{PL}} = 0.15$ denotes a poor emitter, while $Q^0_{\mathrm{PL}} = 0.93$ indicates a good emitter.

It is apparent that Al plasmonics can show a significant enhancement in the quantum yield for emitters with different intrinsic quantum yields when positioned at sub-10 nm distances. Especially for the poor emitter with $Q^0_{\mathrm{PL}} = 0.15$, a 2.1-fold enhancement peak can be observed. As described in the main text, owing to the 'valley of low loss', the radiative decay channel can dominate its non-radiative counterpart for Al NPs. In contrast, for Au NPs, the modified quantum yield is below one, regardless of the value of Q^0_{PL} for the emitter. This suggests that the presence of Au NPs in close

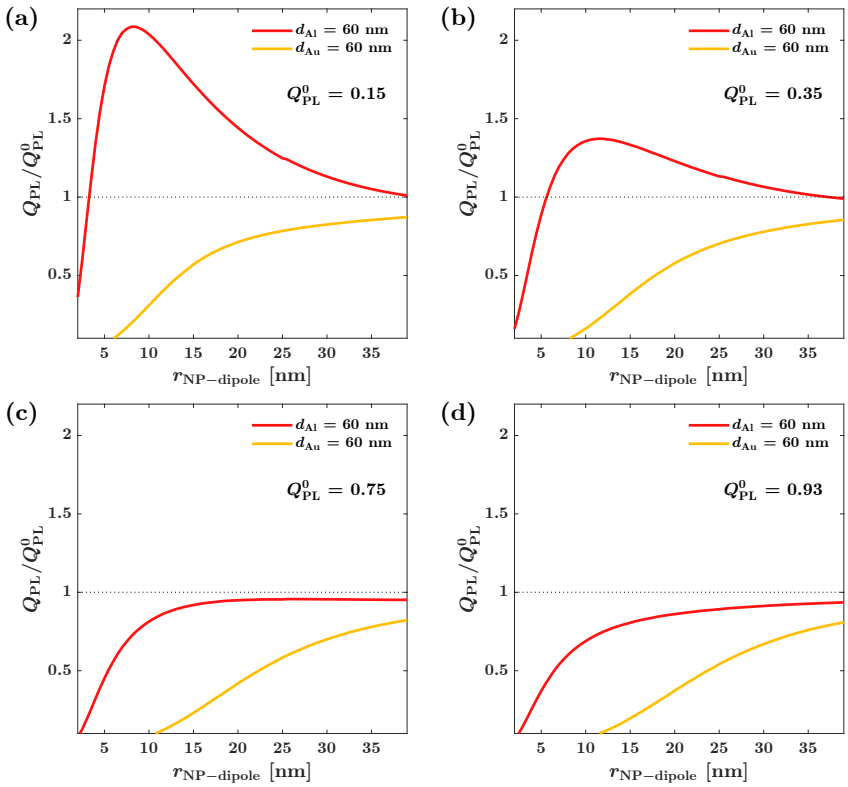

Fig. S1 Modified quantum yield as a function of the distance between the dipole emitter and the NP surface ($r_{\mathrm{NP-dipole}}$) for various intrinsic quantum yields, Q^0_{PL}.

proximity to the emitter can quench the light, rather than enhancing its radiation. This is due to the dominant non-radiative decay channels associated with Au NPs.

S3 Decay rates of core *vs.* core@shell Al NPs

The exact solutions can be extended to the case of core@shell NPs using the transfer matrix (T-Matrix) method. The T-matrix formalism for multilayer concentric spherical NPs was developed by Moroz and his coworkers[8–10]. We adopted this method to account for the presence of an Al_2O_3 shell enveloping the Al nanosphere.

In Figure S2, we compare the distance-dependent and spectral-dependent decay rates between Al NPs under two conditions: core only and core@shell. The calculations were performed with an NP size selected to match the dipole emission wavelength at 485 nm. As shown in the figure, almost the same behavior is observed in both configurations, with the core-only NP configuration exhibiting slightly higher decay rates.

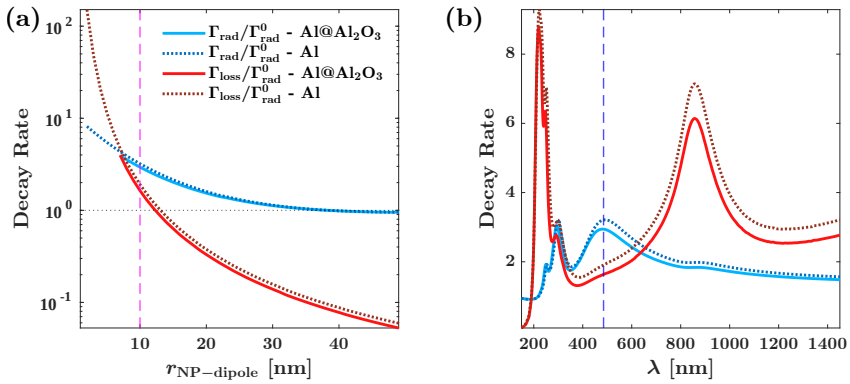

Fig. S2 Radiative and non-radiative decay rates for a 63 nm-diameter Al NP and a 73 nm-diameter Al@Al_2O_3 NP (with the addition of a 5 nm-thick Al_2O_3 shell) as a function of (a) the emitter position from the NP surface and (b) wavelength.

S4 Quasi-static approximations

In this section, we provide detailed analytical expressions as the basis for the simplified equation presented in the main paper (Eq. 1). To offer a more intuitive understanding of the underlying physics, we subsequently adopted a simpler model initially introduced by Gerstein and Nitzan, known as the GN model[11]. Using this model, the expressions for $\Gamma_{\rm rad}/\Gamma^0_{\rm rad}$ and $\Gamma_{\rm loss}/\Gamma^0_{\rm rad}$ can be simplified, eliminating the need for the Riccati-Bessel function:

$$\begin{aligned}
\frac{\Gamma^{\perp}_{\rm rad}}{\Gamma^0_{\rm rad}} &= \left|1+\frac{2}{3}\frac{\alpha_1}{r^3}\right|^2 \\
\frac{\Gamma^{\parallel}_{\rm rad}}{\Gamma^0_{\rm rad}} &= \left|1-\frac{1}{3}\frac{\alpha_1}{r^3}\right|^2 \\
\frac{\Gamma^{\perp}_{\rm loss}}{\Gamma^0_{\rm rad}} &= \frac{c^3}{2\omega^3}\left(4\frac{\Im\left[\alpha_1\right]}{r^6}+\sum_{\ell=2}^{\ell_{\rm max}}(\ell+1)^2\frac{\Im\left[\alpha_\ell\right]}{r^{2\ell+4}}\right) \\
\frac{\Gamma^{\parallel}_{\rm loss}}{\Gamma^0_{\rm rad}} &= \frac{c^3}{4\omega^3}\left(2\frac{\Im\left[\alpha_1\right]}{r^6}+\sum_{\ell=2}^{\ell_{\rm max}}\ell(\ell+1)\frac{\Im\left[\alpha_\ell\right]}{r^{2\ell+4}}\right) ,
\end{aligned} \tag{S5}$$

where the multipolar quasi-static polarizability, α_ℓ, is defined by:

$$\alpha_\ell = 3r_{\rm NP}^{2\ell+1}\frac{\varepsilon_{\rm NP}-1}{\left(\frac{2\ell+1}{\ell}\right)+\varepsilon_{\rm NP}-1} . \tag{S6}$$

Although the model was originally developed using a quasi-static approach, it is possible to incorporate the first-order electrodynamic correction, known as the MLWA model[12,13]. This refines the radiative component of the GN model by including the radiation reaction and the dynamic depolarization factor in the expression for the dipolar polarizability ($\ell = 1$)[14]. The modification is achieved by replacing the expression

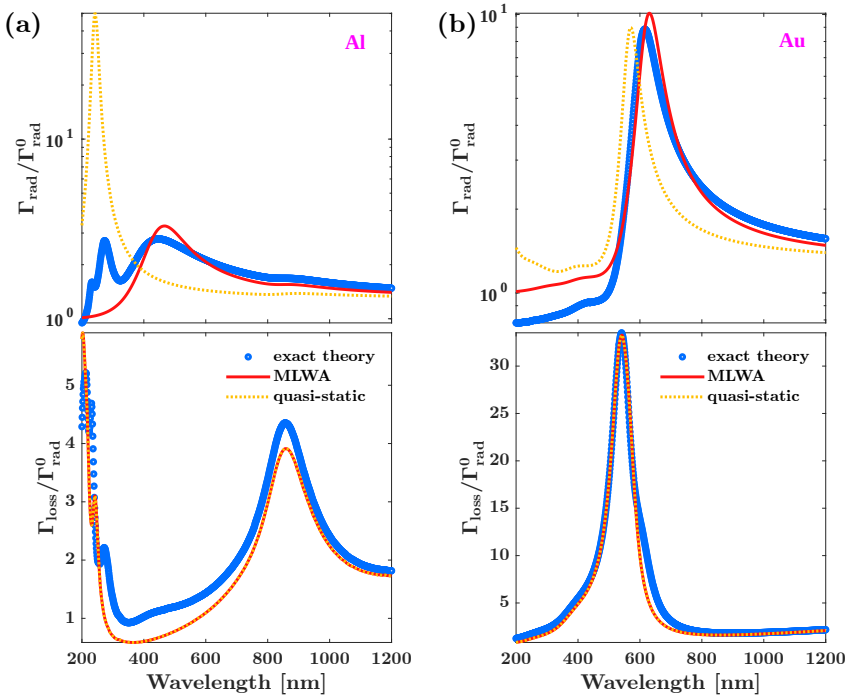

Fig. S3 Comparison of radiative (upper panels) and non-radiative (lower panels) decay rates, showcasing results calculated by exact theory, the modified GN model (MLWA), and the original GN model (quasi-static), for (a) Al and (b) Au NPs with a diameter of 63 nm.

for α_1 in Eq. S6 with:

$$\alpha_1 = L\frac{\varepsilon_{\mathrm{NP}} - \varepsilon_{\mathrm{m}}}{\varepsilon_{\mathrm{m}} + L_{\mathrm{eff}}\left(\varepsilon_{\mathrm{NP}} + \varepsilon_{\mathrm{m}}\right)}\,, \tag{S7}$$

where $L_{\mathrm{eff}} = L - \frac{V}{4\pi r_{\mathrm{NP}}}k^2 - i\frac{V}{6\pi}k^3$ and L represents the static depolarization factor ($L = \frac{1}{3}$ for spherical NPs).

Figure S3 presents a comparison of decay rates derived from both these models and the exact theory for Al and Au NPs, each with a diameter of 63 nm. The GN model aligns well with the exact results for non-radiative decay. In comparison, the modified GN model more closely approximates the exact solutions for the radiation rate than its original counterpart. The deviation observed at shorter wavelengths can be attributed to the analytical approach for the radiative rates, which does not account for high-order multipole components. Nevertheless, these analytical expressions are sufficiently robust to facilitate qualitative predictions, enabling the rapid design and evaluation of decay rate modifications introduced to an emitter by a NP.

S5 Decay rates of NPs using various databases

Figure S4 compares the radiative and non-radiative decay rates of Al and Au NPs across different databases. For Al, the data were sourced from McPeak[6], Rakic[15], and Cheng[16]. For Au, the databases were taken from Babar-Weaver[17], McPeak[6], and

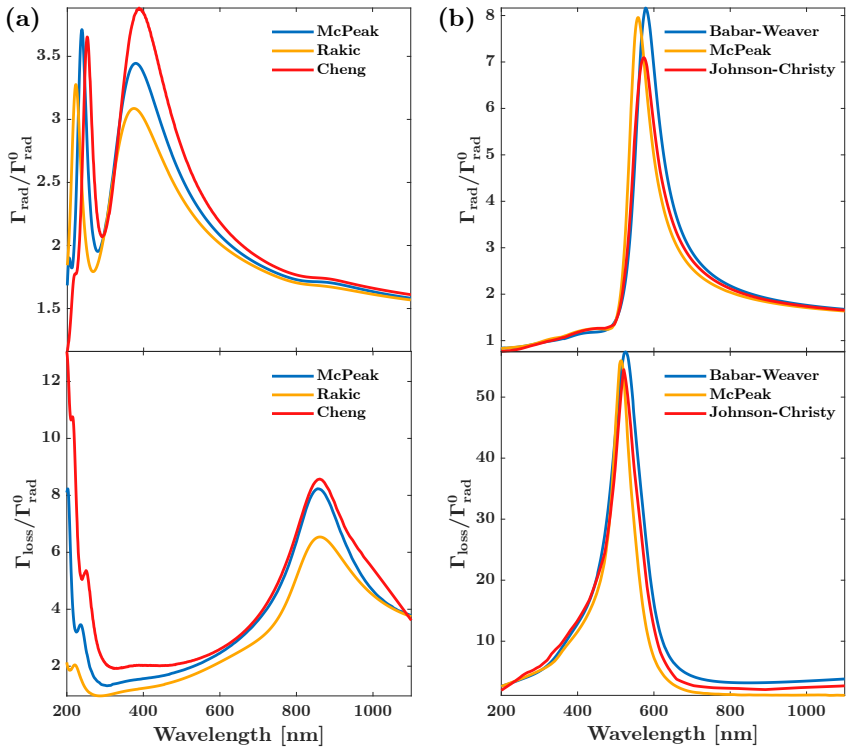

Fig. S4 Radiative (top panels) and non-radiative (bottom panels) decay rates as a function of wavelength for (a) Al and (b) Au NPs with a diameter of 63 nm, calculated based on different databases.

Johnson-Christy[7]. Despite the data coming from various sources, the same spectral lines were observed, indicating that the radiative and non-radiative decay rate features described in the main text do not depend on the specific database selected.

S6 Decay rates of non-spherical NPs: Boundary element method (BEM)

Since the exact theory is limited to spherical particles only, we used the boundary element method (BEM) to simulate decay-rate enhancement for non-spherical NPs[18]. For this purpose, the MNPBEM Matlab toolbox[19] was employed. Prior to the calculations, we calibrated the BEM results by comparing them with those obtained from the exact theory using spherical particles. Figure S5 shows the simulation results for different triangular meshes, where the number of vertices along the spherical azimuth angle (V_ϕ) varied from 10 to 40, while the number of vertices along the spherical polar angle (V_θ) was set to 10. We found that increasing the number of vertices in the direction of the dipole position (V_ϕ) enhances accuracy and numerical stability more effectively, particularly for simulations involving dipoles located closer to the NP surface (see Figure S5c).

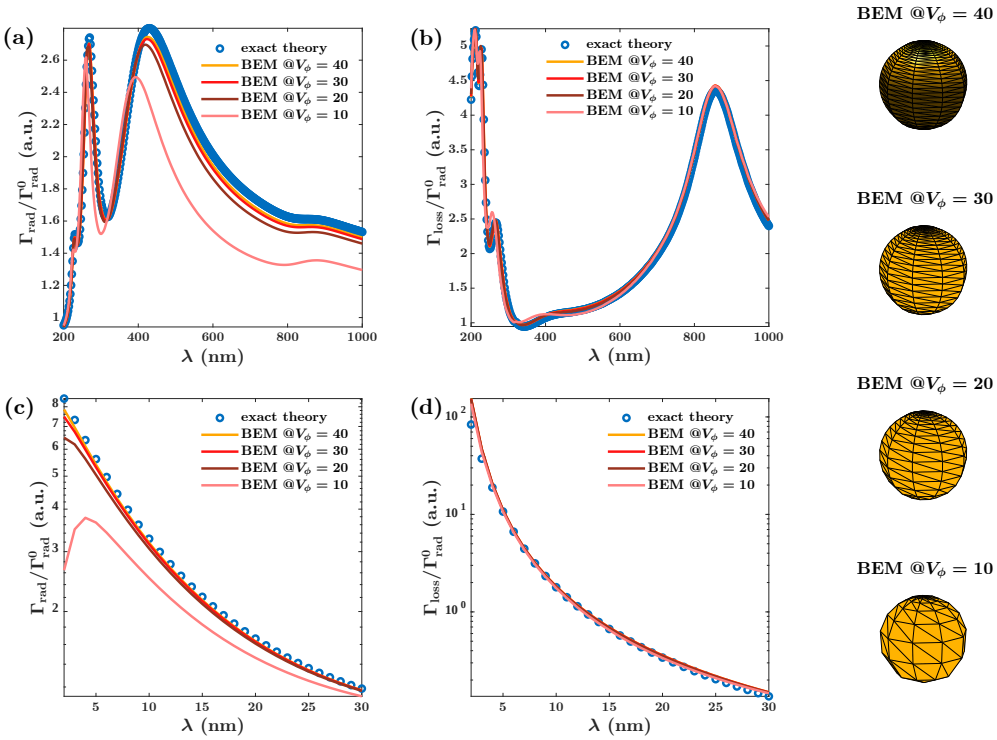

Fig. S5 Comparison of (a, c) radiative decay rates and (b, d) non-radiative decay rates as functions of wavelength and NP emitting distance, respectively, to calibrate BEM calculations to the exact theory. Inset: illustration of the mesh changes on the spherical particle when V_θ is varied.

Figure S6 details the shape of the spectral lines for the radiative and non-radiative decay rates of non-spherical NPs (nanocube, nanorod, and nanodisk) of varying sizes to support the results shown in Figure 2d of the main text. For the nanocube, the side length was varied from 20 nm to 70 nm. For the nanodisk, the thickness was set to 20 nm, and the diameter was varied from 20 nm to 70 nm. Finally, for the nanorod, the diameter was set to 40 nm, and the length was varied from 40 nm to 70 nm.

S7 Experimental extinction efficiency of the Al nanodisk arrays with and without the F8BT emitting layers

Figure S7 presents the extinction spectra of the Al nanodisks, both bare and coated with the F8BT layer, as measured using a custom-built ultraviolet-visible system (refer to the Materials and methods section in the main text for details). The figure demonstrates that the addition of the emitting material atop the samples induces a redshift in the spectrum and a reduction in extinction efficiency.

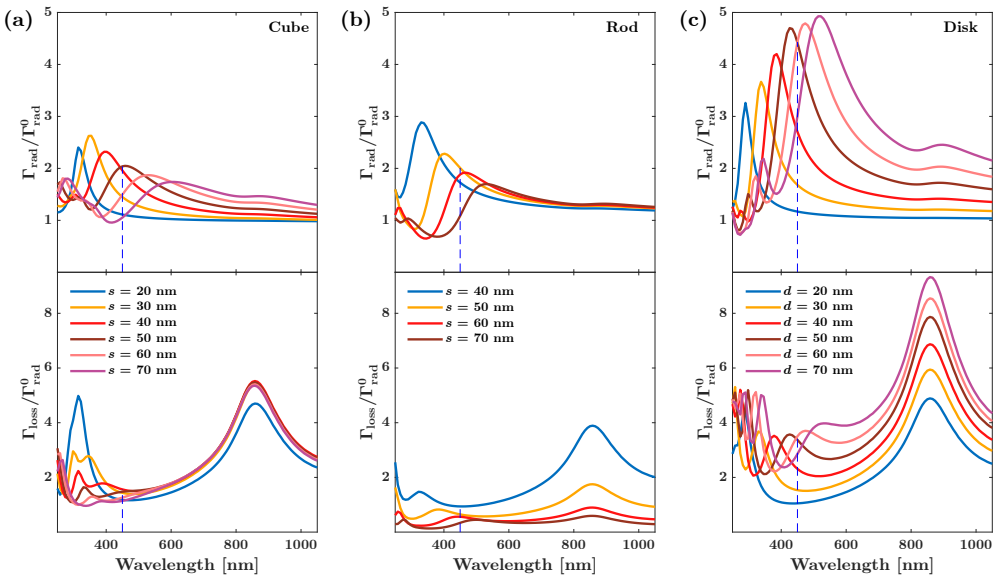

Fig. S6 Radiative (upper panels) and non-radiative (lower panels) decay rates as a function of wavelength for (a) nanocubes, (b) nanorods, and (c) nanodisks with varying sizes (s) or diameters (d).

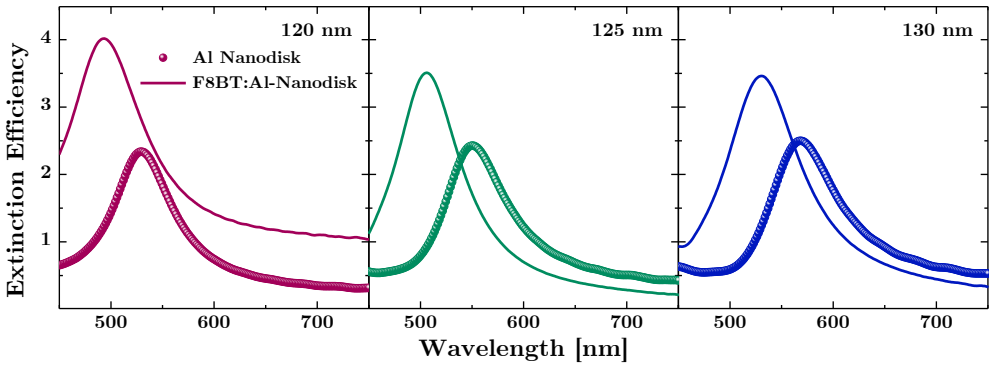

Fig. S7 Experimental extinction spectra of Al nanodisk arrays with varying nanodisk diameters, both without and with a coating of the F8BT emitting material.

References

[1] Ruppin, R. Decay of an excited molecule near a small metal sphere. *J. Chem. Phys.* **76**, 1681–1684 (1982).

[2] Kim, Y. S., Leung, P. & George, T. F. Classical decay rates for molecules in the presence of a spherical surface: A complete treatment. *Surf. Sci.* **195**, 1 – 14 (1988).

[3] Liu, B. *et al.* Feasibility of using bimetallic Au-Ag nanoparticles for organic light-emitting devices. *Nanoscale* **13**, 12164–12176 (2021).

[4] Bohren, C. F. & Huffman, D. R. *Absorption and Scattering of Light by Small Particles* (Wiley, New York, 1983).

[5] Allardice, J. R. & Ru, E. C. L. Convergence of Mie theory series: Criteria for far-field and near-field properties. *Appl. Opt.* **53**, 7224–7229 (2014).

[6] McPeak, K. M. *et al.* Plasmonic films can easily be better: Rules and recipes. *ACS Photonics* **2**, 326–333 (2015).

[7] Johnson, P. B. & Christy, R. W. Optical constants of the noble metals. *Phys. Rev. B* **6**, 4370–4379 (1972).

[8] Rasskazov, I. L., Carney, P. S. & Moroz, A. STRATIFY: A comprehensive and versatile MATLAB code for a multilayered sphere. *OSA Continuum* **3**, 2290–2306 (2020).

[9] Rasskazov, I. L., Moroz, A. & Carney, P. S. Electromagnetic energy in multilayered spherical particles. *J. Opt. Soc. Am. A* **36**, 1591–1601 (2019).

[10] Moroz, A. A recursive transfer-matrix solution for a dipole radiating inside and outside a stratified sphere. *Ann. Phys.* **315**, 352–418 (2005).

[11] Gersten, J. & Nitzan, A. Spectroscopic properties of molecules interacting with small dielectric particles. *J. Chem. Phys.* **75**, 1139–1152 (1981).

[12] Kelly, K. L., Coronado, E., Zhao, L. L. & Schatz, G. C. The optical properties of metal nanoparticles: The influence of size, shape, and dielectric environment. *J. Phys. Chem. B* **107**, 668–677 (2003).

[13] Meier, M. & Wokaun, A. Enhanced fields on large metal particles: Dynamic depolarization. *Opt. Lett.* **8**, 581–583 (1983).

[14] Januar, M. *et al.* Role of depolarization factors in the evolution of a dipolar plasmonic spectral line in the far- and near-field regimes. *J. Phys. Chem. C* **124**, 3250–3259 (2020).

[15] Rakić, A. D., Djurišić, A. B., Elazar, J. M. & Majewski, M. L. Optical properties of metallic films for vertical-cavity optoelectronic devices. *Appl. Opt.* **37**, 5271–5283 (1998).

[16] Cheng, F. *et al.* Epitaxial growth of atomically smooth aluminum on silicon and its intrinsic optical properties. *ACS Nano* **10**, 9852–9860 (2016).

[17] Babar, S. & Weaver, J. H. Optical constants of Cu, Ag, and Au revisited. *Appl. Opt.* **54**, 477–481 (2015).

[18] García de Abajo, F. J. & Howie, A. Retarded field calculation of electron energy loss in inhomogeneous dielectrics. *Phys. Rev. B* **65**, 115418–115434 (2002).

[19] Hohenester, U. & Trügler, A. MNPBEM - a matlab toolbox for the simulation of plasmonic nanoparticles. *Comput. Phys. Commun.* **183**, 370–381 (2012).